









RESEARCH ARTICLE

10.1029/2018JE005740

A Seasonally Recurrent Annular Cyclone in Mars Northern Latitudes and Observations of a Companion Vortex

Key Points:

- We study the Mars seasonal annular cyclone and related phenomena at 60°N and 90°W at $L_s = 120^\circ$ from 1995 to 2018
- The cyclone is accompanied by a second structure, an annular vortex in 2006, 2008, and 2012, and an accompanying cloudy area other years
- We show the wind field and cloud altitudes in 2012. Water ice clouds grow in the morning and weaken and dissipate as the sol advances

A. Sánchez-Lavega¹ , A. Garro¹, T. del Río-Gaztelurrutia¹ , R. Hueso¹, I. Ordoñez-Etxeberria¹, H. Chen Chen¹ , A. Cardesín-Moinelo² , D. Titov³, S. Wood⁴, M. Almeida⁵ , A. Spiga^{6,7} , F. Forget⁶, A. Määttänen⁸ , H. Hoffmann^{9,10}, and B. Gondet¹¹ 

¹Departamento Física Aplicada I, EIB, Universidad del País Vasco UPV/EHU, Bilbao, Spain, ²European Space Agency, ESAC, Madrid, Spain, ³European Space Agency, ESTEC, Noordwijk, Netherlands, ⁴European Space Agency, ESOC, Darmstadt, Germany, ⁵Dias Almeida Data Processing and Systems, Ittigen, Switzerland, ⁶Laboratoire de Météorologie Dynamique (IPSL), Sorbonne Université, Centre National de la Recherche Scientifique, École Polytechnique, École Normale Supérieure, Paris, France, ⁷Institut Universitaire de France, Paris, France, ⁸LATMOS/IPSL, UVSQ, Sorbonne Université, CNRS, Paris, France, ⁹German Aerospace Center (DLR), Institute of Planetary Research, Berlin, Germany, ¹⁰Deceased 19 September 2018, ¹¹Institut d'Astrophysique Spatiale, CNRS/University Paris Sud, Orsay, France

Correspondence to:

A. Sánchez-Lavega, agustin.sanchez@ehu.eus

Citation:

Sánchez-Lavega, A., Garro, A., del Río-Gaztelurrutia, T., Hueso, R., Ordoñez-Etxeberria, I., Chen Chen, H., et al. (2018). A seasonally recurrent annular cyclone in Mars northern latitudes and observations of a companion vortex. *Journal of Geophysical Research: Planets*, 123. <https://doi.org/10.1029/2018JE005740>

Received 27 JUN 2018
Accepted 15 OCT 2018
Accepted article online 19 OCT 2018

Author Contributions:

Conceptualization: A. Sánchez-Lavega
Formal analysis: A. Sánchez-Lavega
Investigation: A. Sánchez-Lavega
Methodology: A. Sánchez-Lavega
Resources: A. Sánchez-Lavega
Validation: A. Sánchez-Lavega
Writing - original draft: A. Sánchez-Lavega
Writing - review & editing: A. Sánchez-Lavega

Abstract We study a seasonally recurrent cyclone and related cloud phenomena observed on Mars at $L_s \sim 120^\circ$, latitude $\sim 60^\circ\text{N}$, and longitude 90°W from images obtained with cameras in different spacecraft between 1995 and 2018. A remarkable double cyclone formed in 2012 and we present a detailed study of its dynamics using images from Mars Express and Mars Reconnaissance Orbiter obtained between 6 June and 9 July. A double cyclone was also observed in 2006 and 2008. In other Martian years the primary cyclone showed an annular cloud morphology with a large water ice cloud observed eastward of it. The cyclones have a size of $\sim 600\text{--}800$ km with a cloud-free core of a radius $\sim 100\text{--}300$ km. Tangential velocities measured from cloud tracking in 2012 images are $\sim 5\text{--}20$ m/s^{-1} at 10-km altitude and double cyclone moved eastward with a velocity of 4 m/s^{-1} during its lifetime of one month. The vortices grow in the morning hours, but with the increasing insolation as the sol progresses, a part of the clouds evaporate, the winds weaken, and the vortices lose coherence. This phenomenon forms under high-temperature gradients in a region with a large north-south topographic slope and has been recurrent each Martian year between 1995 and 2018. We argue the interest of studying its changing properties each Martian year in order to explore their possible relationship to the state of the Martian atmosphere at $L_s \sim 120^\circ$.

Plain Language Summary We study a remarkable annular vortex observed some years to be formed by two coupled cyclones that grow every Martian northern summer at the same longitude and latitude of the planet. Each vortex has a size of 700 km and its center is a cloud-free area with a radius of about 200 km. The vortex is formed by water ice clouds at about 10-km altitude where the winds blow with speeds of 5 to 20 m/s. The clouds grow in the morning hours and sublimate as the vortex weakens with increasing insolation. Dynamical models show that the vortex forms in a region with a large north-south terrain slope that combines with north-south temperature gradient. The study mainly uses images taken in 2012, but a survey shows that the vortex recurrently forms every Martian year between 1995 and 2018. This vortex system can be used as a proxy, studying its variability, to characterize the state of the atmosphere at the time of its formation.

1. Introduction

Transient synoptic eddies, spiral and annular weather systems in the Martian atmosphere, have been reported from images taken by Mariner 9 (Briggs & Leovy, 1974), Viking Orbiter 1 (Hunt & James, 1979) and Mars Global Surveyor (MGS; Cantor et al., 2002; Wang & Fisher, 2009; Wang & Ingersoll, 2002). They form profusely in both hemispheres and at different seasons when the meridional temperature gradient becomes large and baroclinic conditions develop. Among these transient eddies, an “annular” cloud system that was first reported in 1999 from Hubble Space Telescope (HST) images was then recurrently observed in 2001–2006 by the Mars Observer Camera (MOC) on the MGS orbiter, at the same areographical location (latitude $\sim 60^\circ\text{N}$ and longitude 90°W , northward of Alba Patera) and epoch ($L_s \sim 120^\circ$; Cantor et al., 2002; Malin et al., 2010).

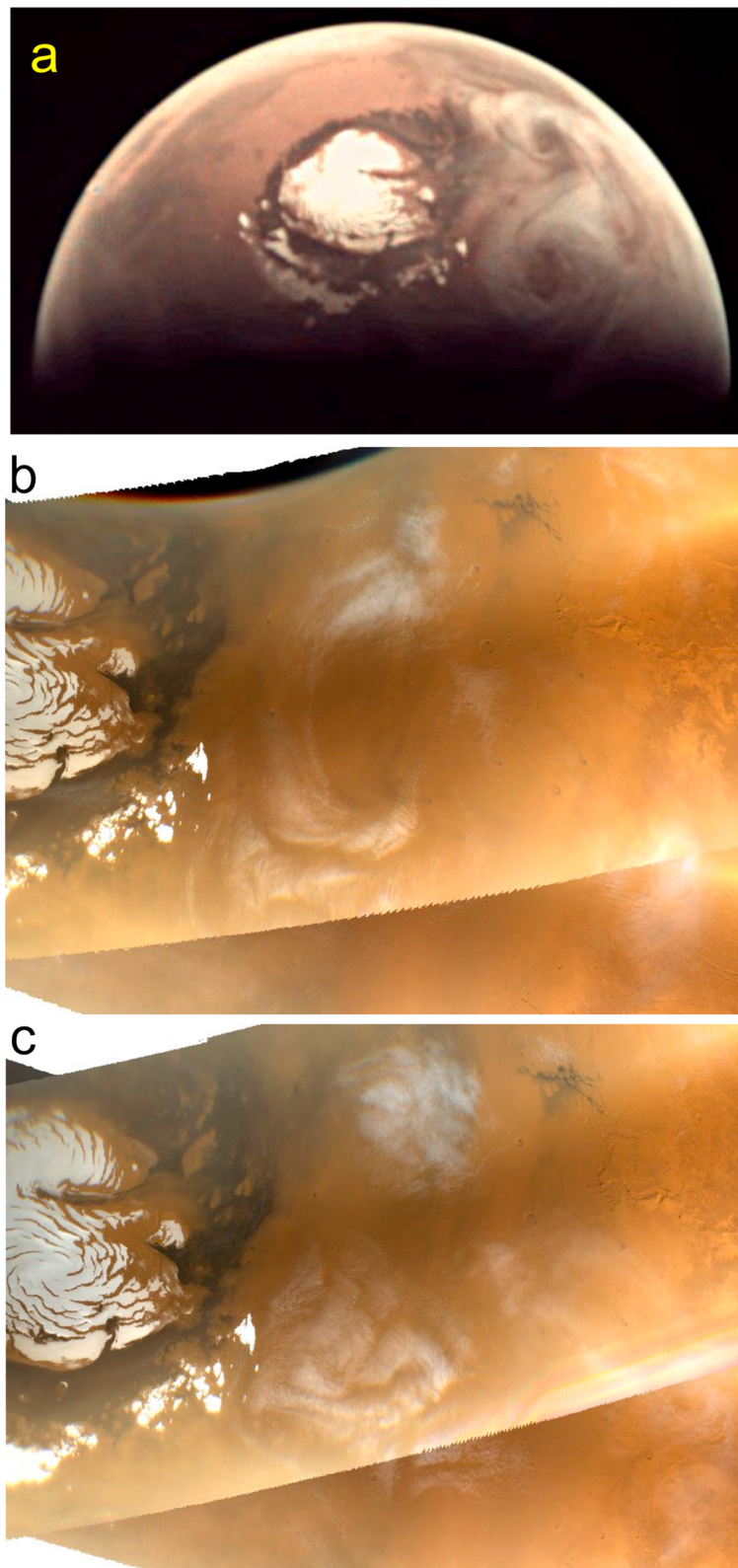


Figure 1. Images of Mars's north pole showing the double cyclone (DC) and the morphology changes in its clouds in June 2012. (a) VMC/MEx 18 June, 03:20 UT (local true solar time, LTST = 8.21 h east vortex, 5.5 h west vortex). (b) Polar projected images of MARCI/MRO 19 June, 12:39:05 UT (LTST = 14.6 h). (c) Polar projected images of MARCI/MRO 20 June, 12:57:34 UT (LTST = 14.9 h).

Images obtained in 2012 with the Visual Monitoring Camera (VMC) onboard Mars Express (MEx) under a favorable polar view, combined with simultaneous images obtained at high-resolution with the Mars Color Imager (MARCI) onboard Mars Reconnaissance Orbiter (MRO) from a nearly equatorial perspective, allowed us to study the annular system in detail. On this year the polar atmosphere developed a remarkable double spiral-annular ring shape with cyclonic vorticity that we call “double cyclone” (from now on double cyclone (DC); Figure 1). Additionally, we have surveyed images of this Mars location and L_s taken with Wide Field Planetary Camera (WFPC2) on Hubble Space Telescope (HST) from 1995 to 1999, MOC/MGS from 1999 to 2006, and MARCI/MRO between 2008 and 2018. We have found that the primary annular vortex is seasonally recurrent, forming each Martian year, and that it is always accompanied by a large cloud of irregular morphology at its east. In 2006 and 2008 the images show the presence of a double vortex similar to the situation observed in 2012. Geographical and climatic conditions probably combine uniquely in the region to generate the system as proposed by numerical models (Tyler & Barnes, 2014). We present here a detailed experimental study of the properties, life cycle, and seasonality of this phenomenon from 1995 to 2018.

2. Properties of the Vortices and Cloud Phenomena

We have used a large set of images obtained in 2012 (Martian year, MY 31) with two different cameras, VMC/MEx (Ormston et al., 2011; Sánchez-Lavega et al., 2018) and MARCI/MRO (Bell et al., 2009; Figure 1) to characterize the DC system in detail. Additionally, we have also used images from MOC/MGS to study the daily cloud behavior of the annular cyclone and its companion eastern phenomenon in 1999, 2001, and 2003 (Malin et al., 1992). The WFPC2 images from HST (1995–1999) were used for early views of the system. Finally, the High Resolution Stereo Camera (HRSC) onboard MEx (Jaumann et al., 2007) and OMEGA/MEx (Bibring et al., 2004) were used to complete the survey of the system with images obtained in 2014 and 2018, respectively. Details on these instruments are given in the supporting information.

VMC images were navigated and orthographically polar projected using the software PLIA (Hueso et al., 2010), and the methods and techniques used are described in detail in Sánchez-Lavega et al. (2018). MARCI and MOC images were calibrated and converted to a navigable format using Integrated Software for Imagers and Spectrometers (ISIS) from the U.S. Geological Survey (<https://isis.astrogeology.usgs.gov/>). They were further analyzed with the QGIS open-source software (<https://www.qgis.org/en/site/>). The daily evolution of features is described using Local True Solar Time (LTST; Allison, 1997).

In this section, we use images of 2012 to study the double vortex in detail, showing among other things, its cyclonic character and fast evolution along a sol. In addition, in some other Martian years the eastern large cloud area has been observed to have a similar morphology to the annular cloud (western cyclone), also displaying a well-developed central eye. In those cases, in analogy with the situation in 2012, we identify this large cloud with a cyclone, thus forming a double cyclone (DC hereafter). This was the case in 2006 and 2008 (MY 28, 29; see below). Other years, the main annular cloud was accompanied to the east by a large cloud feature with no eye visible. However, given the rapid daily evolution observed in 2012 (Figures 1 and 2), and the limited temporal coverage of the relevant local times in those Martian years, we cannot exclude the possibility of the transient formation of a DC that has not been observed.

2.1. The 2012 DC Case: Vortices' Size, Motion, and Rotation

Analyzed VMC images cover the period from 6 June to 9 July 2012 ($L_s = 120.8^\circ$ – 136.6° , MY = 31; Table 1 and Figure 2). The first observation of cloud trails at latitude $\sim 60^\circ\text{N}$ and longitude 90°W occurred on 6 June, but a conspicuous vortex with annular shape was detected on 11 June at LTST ~ 6 – 11 h. The vortex developed as a double system during 16–18 June with very pronounced central areas free of clouds (the “eyes”; Figures 1 and 2). The size of the vortices, as traced by the clouds at their approximate outer circular limit, was in the range of 600–800 km. Both vortices show eyes with a radius ~ 75 – 100 km when the DC appears as a compact double vortex, but a larger eye of radius ~ 250 – 350 km develops later in the sol when the DC evolves to a single and broken vortex (see Figure 1b and section 3.2). The separation between vortex centers was $\sim 45^\circ$ in longitude ($\sim 1,330$ km), equivalent to a zonal wave number 4 if we assume that this distance corresponds to a half-wavelength along the latitude circle. Between 15 and 23 June, the vortex centers moved eastward with a speed of ~ 3 – 5 m/s^{-1} while oscillating around latitude 55° – 65°N (Table 1 and Figure 3). By 2 July, the DC spiral shape vanished, and the last cloud trails disappeared before 9 July.

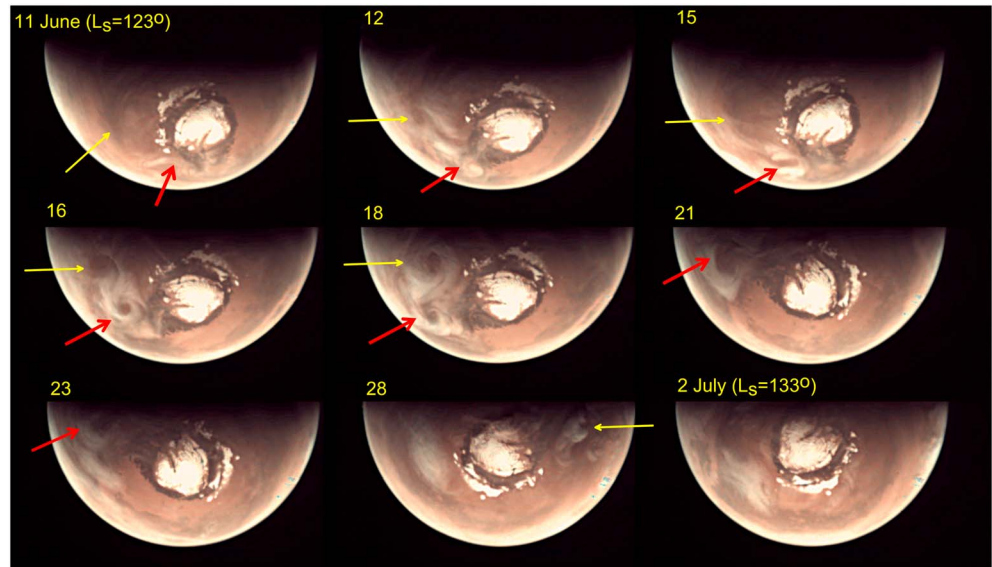


Figure 2. Images from VMC-MEx showing the evolution of the double-vortex along 20 Earth days from 11 June to 2 July 2012 (dates indicated on the top). The red arrow marks the preceding (eastern vortex) and the yellow one the following (western vortex). (top row) Genesis. (middle row) Mature stage. (bottom row) The decay. Data for each image can be found in Table 1.

We have measured the motions of individual clouds in the DC using image pairs obtained by VMC (time separation ~ 16 min) and MARCI (time separation ~ 2 hr), retrieving the wind vectors relative to the center of the vortices (Figure 4). We used two different methods: (a) visual cloud identification and tracking and (b) a supervised brightness cross-correlation velocimetry method (Hueso et al., 2009) adapted to polar coordinates (Garate-Lopez et al., 2013). The velocity vectors reveal cyclonic (counterclockwise) rotation of both vortices with tangential velocities in the range $V = 5\text{--}20$ m/s $^{-1}$. We derived peak vorticities of $\xi \sim \partial u/\partial y - \partial v/\partial x \sim 4 \times 10^{-5}$ s $^{-1} \sim 0.3 f$, where $f = 2 \Omega \sin \varphi = 1.2 \times 10^{-4}$ s $^{-1}$ is the Coriolis parameter at latitude $\varphi = 60^\circ\text{N}$ ($\Omega = 7.08 \times 10^{-5}$ s $^{-1}$ is the planet angular velocity). Taking $V = 15$ m/s $^{-1}$ and $R = 300$ km as characteristic velocity and length, the Rossby number $Ro = V/fR \sim 0.4$ indicates that the cyclones are in gradient wind balance (Sánchez-Lavega, 2011).

$$\frac{V^2}{r} + fV = \left| \frac{1}{\rho} \frac{\partial P}{\partial r} \right| \quad (1)$$

The depth of the low-pressure centers (implied by cyclonic motion) can be estimated from equation (1) using the above values for V and R and a mean atmospheric density $\rho = 0.018$ kg/m 3 , yielding a radial gradient

Table 1

Location of The Double Vortex in 2012 From VMC/MEx and MARCI/MRO

Data	Eastern Vortex						Western Vortex			
	Number	Date, UTC Time	Sol	Instrument	LTST	Longitude W.	Latitude	LTST	Longitude W.	Latitude
1	15/06/2012, 05:26:12	269	VMC	11.03	85.5	65.6	-	-	-	-
2	16/06/2012, 02:24:30	270	VMC	07.85	71.2	61.7	05.91	100.0	55.8	
3	17/06/2012, 12:02:10	271	MARCI	14.60	65.2	60.5	15.05	97.2	59.1	
4	18/06/2012, 03:20:30	272	VMC	08.21	56.4	56.6	05.51	102.3	61.4	
5	18/06/2012, 12:20:36	272	MARCI	15.51	50.1	58.2	14.90	98.9	63.1	
6	19/06/2012, 12:39:05	273	MARCI	15.93	44.8	58.9	14.61	92.3	62.3	
7	20/06/2012, 12:57:34	274	MARCI	16.03	38.5	58.8	13.36	83.4	62.1	
8	21/06/2012, 01:15:00	275	VMC	05.78	36.2	54.3	03.98	49.9	59.7	
9	23/06/2012, 02:11:06	277	VMC	06.08	22.8	58.4	04.88	40.0	53.8	

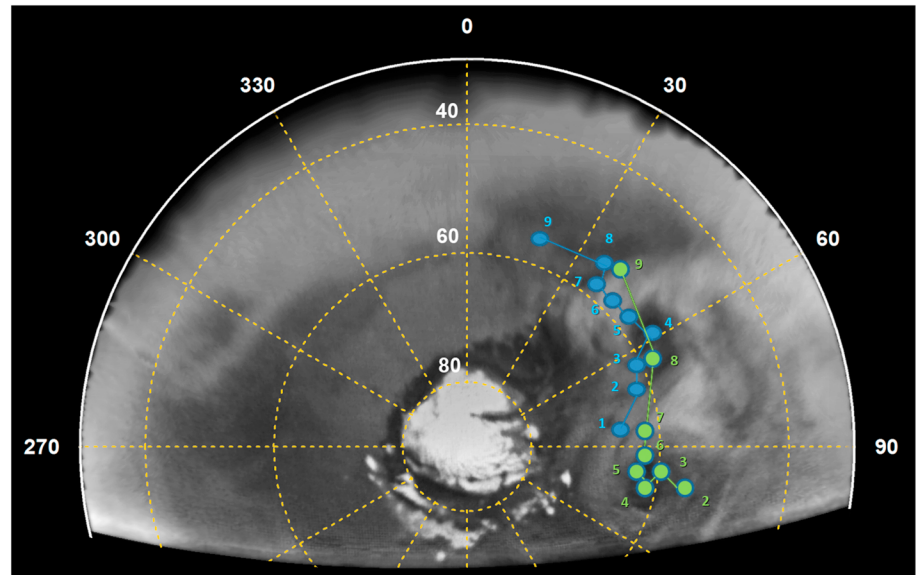


Figure 3. Motion of the center of each vortex of DC in June 2012 superimposed to a north polar projection from 18 June. Blue dots show the location for the eastern vortex and green dots the western one. West longitudes and latitudes are indicated by dotted lines. Date and time corresponding to each vortex location (from 1 to 9) are given in Table 1.

pressure $\partial P/\partial r \sim 5 \times 10^{-4}$ mbar/km and a difference between the center and edge of 0.2 mbar. This is about 2 orders of magnitude lower than the standard for Earth's extratropical cyclones (Sánchez-Lavega, 2011), an expected result due to the lower density of the Martian atmosphere as compared to Earth and proportional to the Martian atmospheric pressure. This result is also in agreement with that obtained by Hunt and James (1979) for similar Martian spiral vortices.

2.2. Water Ice-Cloud Types and Altitude of Clouds

The altitude of the clouds in the DC has been derived from the shadows projected on the surface on high-resolution MARCI images (Figure 5). Given x , the measured horizontal projected distance between the cloud and its shadow, and i , the solar incidence angle, we can estimate the cloud altitude above surface as $h = x/\tan i$. Using different measurements, we obtain $h = 10 \pm 3$ km, a result that agrees with the altitude measurements on other vortices (Hunt & James, 1979).

VMC and MARCI color images show that the vortex clouds are white, suggesting that they are water ice condensates (Figures 1 and 4). The images do not indicate the presence of dust, which would introduce nondetected yellowish color patterns. We have retrieved the pressure-temperature and water vapor mixing ratio profiles at the longitude and latitude of DC for the appropriate LTST and L_s from the Mars Climate Database (MCD; Forget et al., 1999; Millour et al., 2015), based on Global Climate Modeling including the Martian water cycle (Navarro et al., 2014), and we have compared them with the CO_2 and H_2O vapor pressure saturation curves (Figure 6). We find that water ice, but not CO_2 , can condense in the altitude range 8–15 km, in full consistency with the retrieved altitude measurements.

The cloud field of DC shows a rich morphological variety that reflects the subjacent dynamical mechanisms at work. This morphology evolves rapidly from hour to hour and from sol to sol (Figure 7). During the DC mature stage, the dominant cloud structures are the spiral bands and arcs that trace each vortex, with lengths ~ 500 – $1,000$ km, reminiscent of the frontal bands of terrestrial extratropical cyclones. There are also fields of mesoscale waves with wavelengths ~ 20 – 25 km, probably gravity waves signaling stable atmospheric conditions. Other different cloud types (Houze, 2014) that can be identified are thin cirrus with low optical depths, thicker and massive stratified clouds, and compact cluster cell areas that resemble altocumulus fields (see also Figure 8). On Earth, altocumulus clusters form in a thin layer where cellular moist convection is driven by Rayleigh-Bénard instability, and the horizontal size of a single cell is about 2 times the layer thickness, which is typically one scale-height or less. In the DC, the cells have a diameter of 5–15 km, close to the scale-height

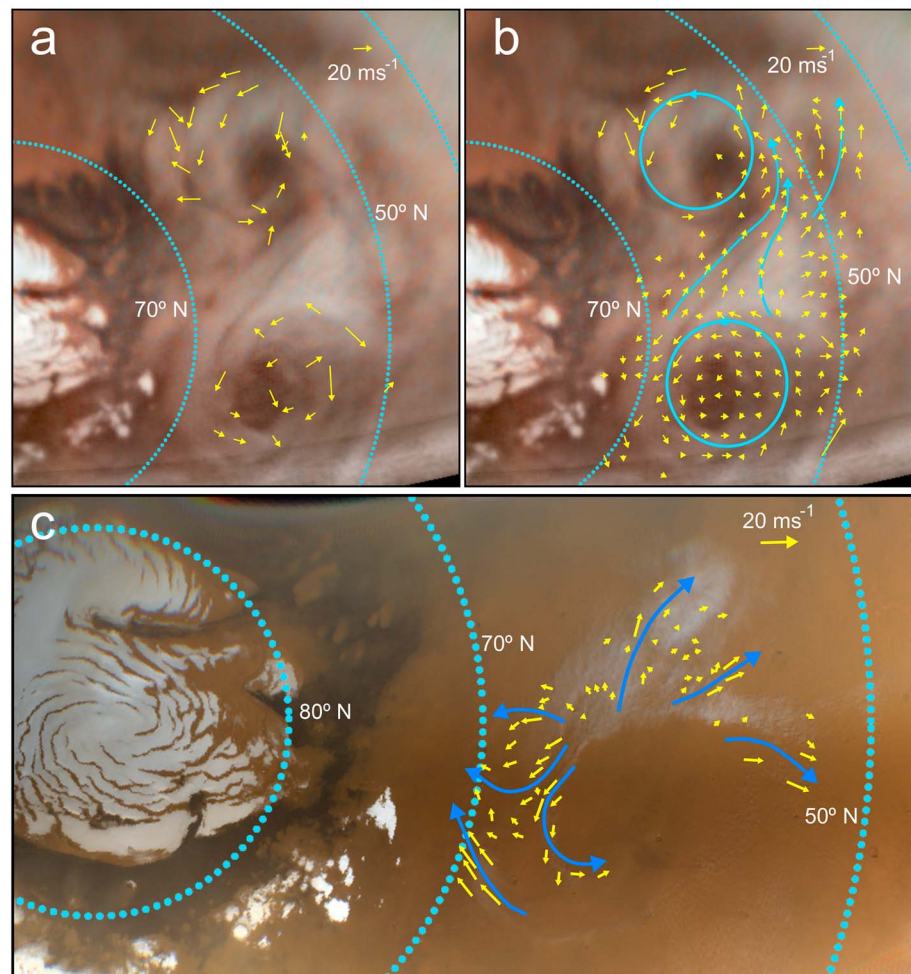


Figure 4. Wind velocity field on DC measured at different LTST in 2012. VMC/MEx images on 16 June 2012 with vortices centers at LTST 5.91 h (eastern) and 7.85 h (western) using (a) manual tracking and (b) supervised brightness cross-correlation velocimetry method. (c) MARCI/MRO image on 17 June 2012 showing the western vortex weakening at 15.05 h LTST. The blue lines trace the approximate flow direction.

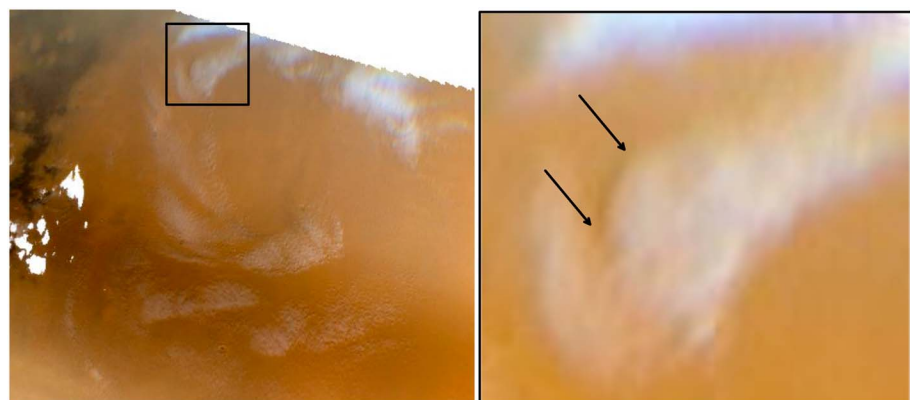


Figure 5. Cloud shadow from (a) MARCI/MRO image taken 19 June 2012 (14:31:14 UT) at right, the augmented image showing the projected shadow along the edge of dense clouds.

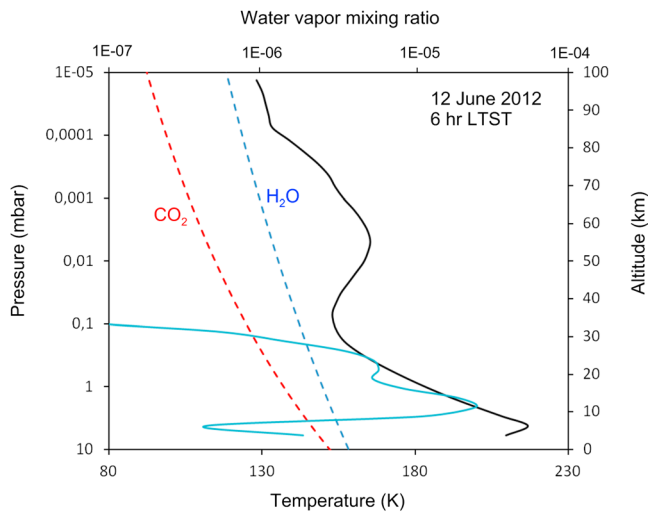


Figure 6. Vertical profiles of temperature (black line) and water vapor mixing ratio (cyan continuous line) for 12 June 2012 according to the Mars climate database (MCD), and saturation vapor pressure for H₂O and CO₂ (dashed labeled lines; Sánchez-Lavega, 2011).

$H = 8\text{--}10$ km for temperatures $T = 160\text{--}200$ K. In the Martian atmosphere, latent heat release within water-ice clouds is negligible, and thus, moist convection does not occur. However, convective motions within clouds are still possible from late afternoon to early morning due to the radiative impact of water-ice crystals (Madeleine et al., 2012; Spiga et al., 2017; Wilson et al., 2007), which could lead to the observed cellular structures in the horizontal dimension.

Figure 8 shows the evolution of the cloud field over three consecutive days and approximately at the same local time, along a strip extending north and south of the central eye of the annular vortex as observed in 2018. A lumpy texture of the cloud field can also be seen north of the central eye. It can also be noticed a drift in longitude of the central region (shown partially) that is largely devoid of clouds in comparison to the annular region.

2.3. Evolution Cycle of the Phenomenon Along a Sol

As it can be seen in Figures 1, 2, and 8–14, there are rapid changes with LTST even over short time periods. Rapid changes occur in both situations: when we observe a double vortex and in the case of an annular vortex with the eastern companion cloud area (see also Cantor et al., 2002). In Figures 9 and 10, we show early views of the annular vortex and eastern cloud obtained with HST in 1995–1999 (MY = 22–24). These figures also

illustrate several instances of the evolution of the system along a sol: Figures 9b and 9c show the change of the two components of DC in ~ 7.3 hr from morning to evening ($L_s = 119.5^\circ$) and Figures 9d–9f, the evolution in ~ 6.5 hr from morning to noon ($L_s = 139^\circ$) in MY 23. Similarly, in Figure 10, we show the DC morphology and its evolution in about ~ 6.5 hr in MY 24 ($L_s = 130.5^\circ$).

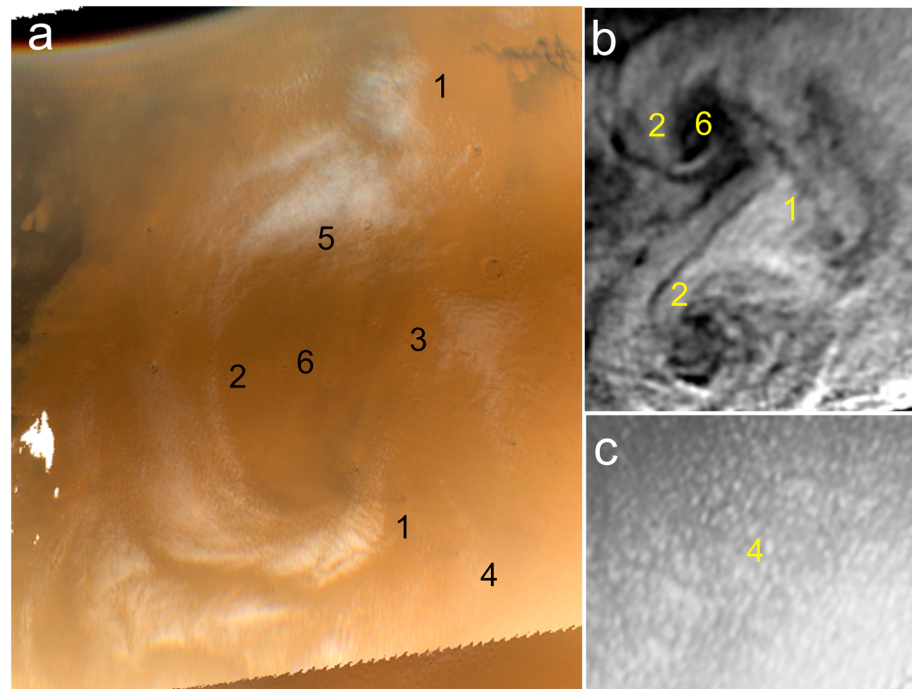


Figure 7. Diverse cloud morphology types in DC in 2012: (1) gravity waves; (2) arc-spiral bands; (3) cirrus-like field; (4) altocumulus cloud field (enlarged in inset (c)); (5) thick stratus-like clouds; and (6) the eyes of DC, free of clouds. (a) 19 June 2012 (LTST = 15.5 hr), MARCI/MRO. (b) 18 June 2012 (LTST = 5.5 hr (east)–8.2 hr (west)), VMC/MEx. (c) 17 June 2012 (LTST = 15 hr), MARCI/MRO.

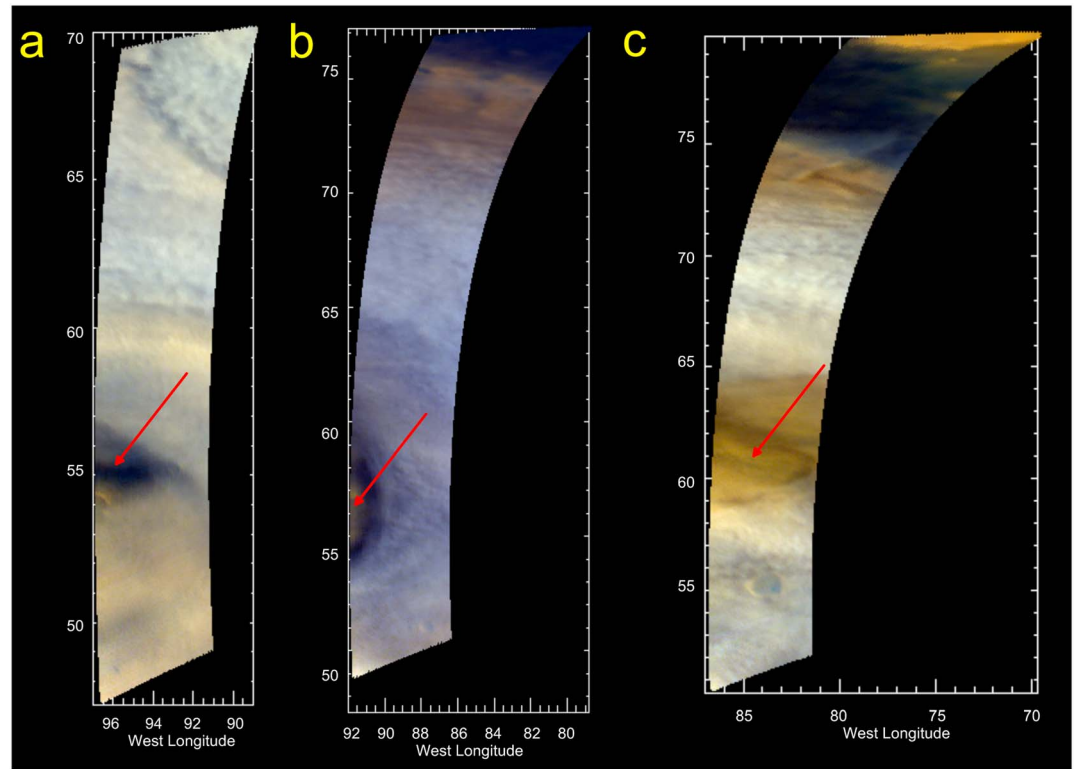


Figure 8. Images from OMEGA-Mex with snapshots of the western cyclone in February 2018, showing the evolution of the clouds over time scales of a few days. (a) 2 February, $L_s = 124^\circ$ (orbit 17825), LTST = 05:00–05:30 hr. (b) 4 February, $L_s = 125^\circ$ (orbit 17842), LTST = 05:00–05:30 hr. (c) 6 February, $L_s = 126^\circ$ (orbit 17849), LTST = 05:00–05:30 hr. Composite RGB (stretched) at R (900 nm), G (650 nm), and B (450 nm). The arrow marks the central eye drift and cloud morphology changes.

The coherence and compactness of both components, observed in the morning hours (~6 hr LTST), weakens as the sol progresses (Figures 1, 4, 9, and 10). In 2012, when DC formed, we observed that during the afternoon (~16 hr LTST) broken and fragmented cloud systems are visible with less intense rotation of the clouds (see, for example, Figures 1, 2, and 4c). In other words, with the increasing insolation along a sol, the vortices lose their cores and become a pair of irregular spots due to their weakening by vorticity loss. In addition, the area covered with clouds is smaller during the afternoon than during the morning hours. Due to the night low temperatures, the double vortex recovers and forms again reappearing the next morning. This daily cycle has been observed for several sols in 2012 thanks to the favorable polar viewing angle of VMC (Figure 2).

In order to analyze the evolution of the cloud-covered area of both components as a function of LTST we selected MOC image sequences in 1999, 2001, and 2004 because of their more complete time coverage in LTST (see Figures 11 and 12 and Table 2). In order to measure the cloud-covered area, we used a simple area selector using a polygon drawer tool. The cloudy area was fragmented in polygonal regions, and in each region, we measured the enclosed number of pixels. The number of pixels was then converted to km^2 using image navigation and projection parameters, and finally, all the polygon areas were summed to retrieve the total area of the cloudy region as a function of LTST (Figure 11).

The decrease in the cloud-covered area as the insolation increases can be attributed to water ice sublimation due to increasing temperatures. Assuming that the solar energy deposited by unit time and area is constant, the sublimating ice area A varies with time as

$$A(t) = A_0 e^{-t/\tau} \quad (2a)$$

$$\tau = \frac{Q_S \rho_{\text{H}_2\text{O}} \left(\frac{4}{3} a\right) \tau_{\text{opt}}}{1 - \varpi_0} \quad (2b)$$

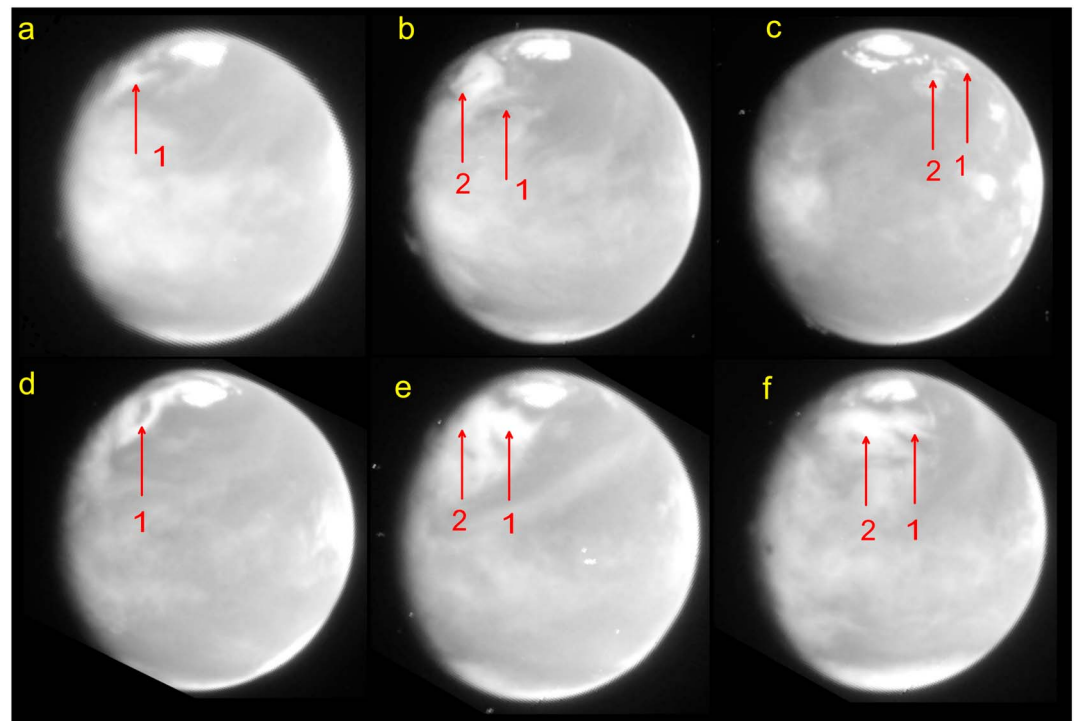


Figure 9. Images of the phenomenon taken with the Hubble space telescope wide field planetary camera (WFPC2) at blue wavelengths (410 nm) in (a) 1995 and (b–f) 1997. The two components of the system are identified with numbers 1 (eastern) and 2 (Western). (a) 6 July 1995 (11 h 23 m 16 s UT). (b) 17 May 1997 (17 h 37 m 20 s UT). (c) 18 May 1997 (2 h 54 m 22 s UT). (d–f) 27 June 1997 (14 h 10 m 14 s UT, 17 h 23 m 14 s UT; 20 h 37 m 14 s UT). More complete data are provided in Table 2. In (a) and (d), the eastern feature (1) shows hints of a core-like structure.

where τ represents a sublimation time constant that depends on the following parameters: the latent heat of sublimation for water ice (Q_s ; Sánchez-Lavega, 2011), water density ($\rho_{\text{H}_2\text{O}} = 1 \text{ g/cm}^3$), ice particle radius (a), particle single scattering albedo (ω_0), and cloud optical depth (τ_{opt}). We have calculated an averaged decreasing cloud area with LTST (a single curve) and fitted it to equations (2a) and (2b) leaving the sublimation time as a free parameter (Figure 12). The best fit is obtained for a sublimation time of $7 \pm 1 \text{ hr}$,

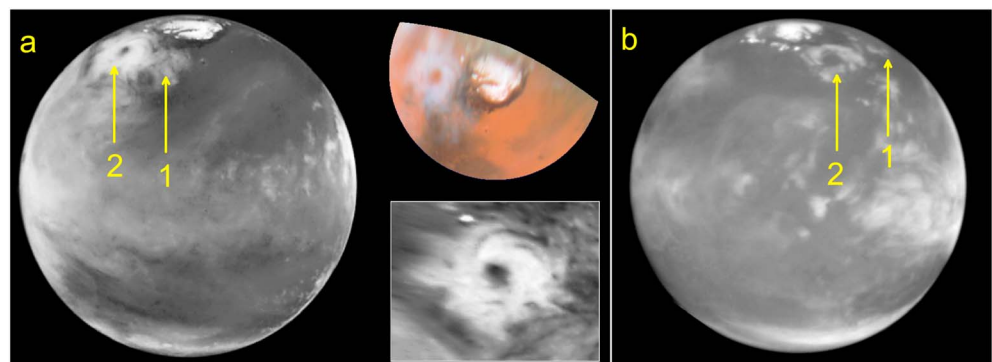


Figure 10. Images of the phenomenon taken with the Hubble space telescope wide field planetary camera (WFPC2) in 1999 at blue wavelengths (410 nm), except for the color polar projection. (a) 27 April 1999 (18 h 13 m 13 s UT), together with a polar projection and a detail of the western annular vortex (2). (b) 28 April 1999 (00 h 40 m 13 s UT). More complete data are provided in Table 2. Credits: Jim Bell (Cornell University), Steve Lee (University of Colorado), Mike Wolff (SSI), and NASA (http://hubblesite.org/news_release/news/1999-22).

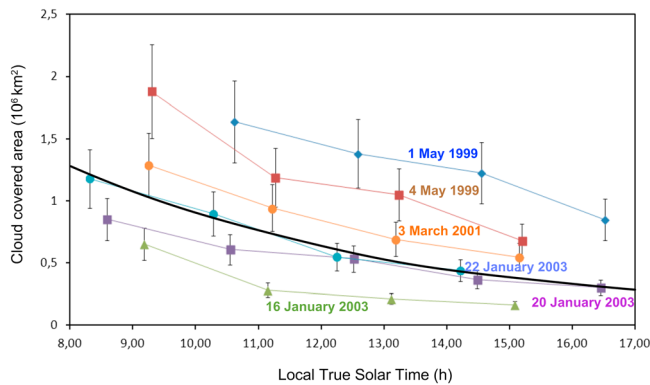


Figure 11. Cloud-covered area evolution with local time on six different sols, measured on MOC/MGS images. Sols correspond to three different Martian years: MY 24 (1–4 May 1999, $L_s = 132^\circ$ – 134°), MY 25 (3 March 2001, $L_s = 123^\circ$), and MY 26 (16–20–22 January 2003, $L_s = 123^\circ$ – 127°). The black curve is the prediction of a model for water-ice sublimation as an explanation for the decreasing cloudy area with increasing insolation.

which implies the following range of values for the parameters (Clancy et al., 2017): $a = 0.1$ – $1 \mu\text{m}$, $\varpi_0 = 0.99$ – 0.999 , and $\tau_{\text{opt}} = 0.1$ – 1 . For larger particles with a volume equivalent radius of $\sim 35 \mu\text{m}$ as measured with the LIDAR onboard Phoenix (Whiteway et al., 2009), optical depths ~ 1 will require less scattering particles with $\varpi_0 = 0.965$.

3. Discussion on the Phenomenon and Formation Mechanism

3.1. Seasonal Recurrence

As stated above, we have searched for the long-term presence and potential double-vortex nature of the phenomenon in images of the region and epoch of interest taken with a battery of instruments (WFPC2/HST, MOC/MGS, MARCI/MRO, and VMC, OMEGA, and HRSC on MEx), spanning the period 1995–2018 (MY = 22 to 34; see Table 2 and Figures 8–10 and 12–14). Remarkably, during this period, the phenomenon has been observed every Martian year forming in the same areographic location ($\sim 60^\circ\text{N}$, $\sim 90^\circ\text{W}$) and at the same season $L_s \sim 120^\circ$. It is therefore annually recurrent, pertaining to the global development of clouds during the Martian aphelion season (Clancy et al., 2017). However, the appearance of the system traced by clouds, and thus its structure and dynamics, shows, as described above, year-to-year variations that might be related to the interannual variability in dust loading in summertime polar regions.

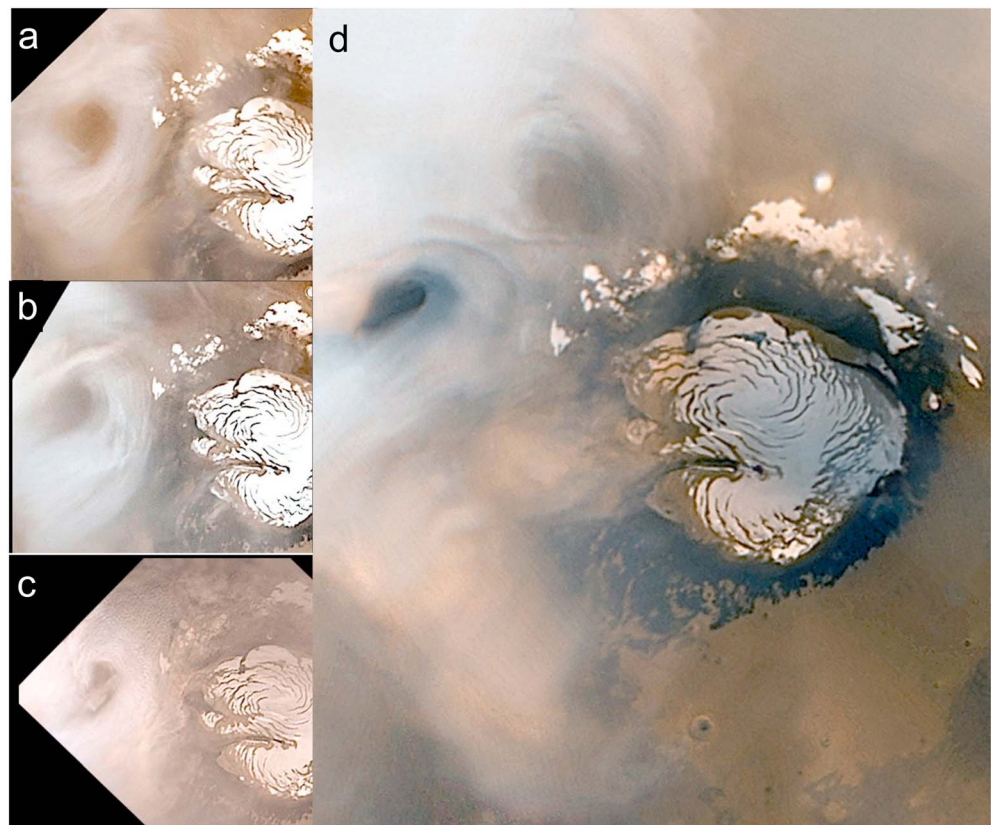


Figure 12. Selected images of DC as seen between 2001 and 2006 obtained with MOC/MGS. (a) 2 March 2001, MY25 $L_s = 124^\circ$. (b) MOC/MGS, 9 January 2003, MY26 $L_s = 120^\circ$. (c) 27 November 2004, MY27 $L_s = 121^\circ$. (d) 14 October 2006, MY28 $L_s = 120^\circ$. Adapted from figures in Malin et al. (2010) and Tyler and Barnes (2014).

Table 2
Long-Term Record of the Phenomenon

Date	Sol	MY	L_s (°)	Instrument
06/07/1995	263	22	122.2	HST
17/05/1997–27/06/1997	257–297	23	119–139	HST
29/04/1999–07/05/1999	281–289	24	131–135	MOC
27/04/1999	280	24	130.5	HST
28/02/2001–28/03/2001	266–293	25	123.6–137.1	MOC
09/01/2003–23/01/2003	259–272	26	120–127	MOC
27/11/2004–27/12/2004	260–289	27	121–135	MOC
14/10/2006	260	28	121	MOC
20/09/2008	278	29	129	MARCI
19/07/2010–11/08/2010	259–281	30	120–131	MARCI
06/06/2012–09/07/2012	260–292	31	120.8–136.6	VMC
17/06/2012–20/06/2012	271–274	31	126.0–127.4	MARCI
01/05/2014–14/05/2014	267–280	32	126.6–130.4	MARCI
02/05/2014–15/06/2014	268–286	32	124.8–133.2	HRSC
07/03/2016–22/03/2017	256–271	33	119.1–126.1	MARCI
09/03/2016–21/03/2016	258–270	33	120–125.6	VMC
25/01/2018–05/03/2018	258–296	34	120–138.8	MARCI ^a
02/02/2018–11/02/2018	266–275	34	124–127.9	OMEGA

^aFrom the MRO MARCI WEATHER REPORT: Malin et al., MRO MARCI Weather Report for the week of 22–28 January 2018, Malin Space Science Systems Captioned Image Release, MSSS-515, http://www.msss.com/msss_images/2018/01/31/. (accessed 2018)

A complete sample of the presence and seasonal aspect of the phenomenon from 1995 to 2018 is shown in Figures 8–10 and 12–14. We have captured the coherent double-vortex nature (DC), with two well-defined cores in 2006 (MY 28; Figure 12d), 2008 (MY29; Figure 13a), and 2012 (MY31; Figures 1, 2, 4, 12c, and 13c). The vortices stand out, as stated above, in the morning hours. In the other years, the phenomenon is characterized by the presence of a well-developed western cyclone, with marked “annular” morphology and core, when still close to the morning side terminator, preceded by an eastern cloudy spot without a clear sign of vorticity (Figures 9, 10, and 12–14). Years in which a very good image sampling and temporal coverage is available show a rapid daily and sol to sol evolution, from compact vortices to irregular cloud spots (Figures 1 and 2). This rapid evolution would make it difficult to capture the double vortex in the absence of good image coverage. Thus, from the available data it is not possible to conclude if the double cyclone formed or not in the years when it was not detected. Hints of a possible double vortex in 2010 are also shown in Figure 13b.

3.2. Footprint at the Phoenix Lander Data

The Phoenix spacecraft landed close to the region of interest at 68°N and 126°W. The mission was active between 26 May and 28 October 2008 (152 sols) encompassing the range $L_s = 76^\circ$ to 148° (Smith et al., 2009). Sols 255 to 283 correspond to $L_s = 118^\circ$ to 133° when the DC developed (see Figure 13a). The west vortex of the pair formed at $\sim 110^\circ$ W and the east vortex at $\sim 70^\circ$ W, and thus, their centers were at about 350 and 1,240 km east of the Phoenix lander, respectively. Since the vortices sizes were 600–800 km their range of action reached the Phoenix area of measurements. Indeed, Holstein-Rathlou et al. (2010) measured a change in the wind speed and direction at sol 100 ($L_s = 123^\circ$), when daytime winds changed from an average 4 m/s^{-1} from the east to $\sim 6\text{--}10 \text{ m/s}^{-1}$ from the west. A few sols before, at sol 94 ($L_s = 120^\circ$), very bright, thick, and fluffy clouds were observed for the first time at midsol with Surface Stereo Imager (SSI; Moores et al., 2010), and similar clouds were present until $L_s = 133^\circ$. These clouds were at mean altitudes of $\sim 5 \text{ km}$, but with clouds at different heights moving at different speeds, with velocities in the range $2\text{--}11 \text{ m/s}^{-1}$. These data are consistent with our measurements and imply the detection of the phenomenon with the instruments on Phoenix.

3.3. Dynamical Interpretation

Several distinct types of atmospheric transient eddies occur in the Martian mid-to-high latitudes. Baroclinic eddies propagate in midlatitudes at winter solstices (Barnes, 1984; Barnes et al., 1993; Hollingsworth et al., 1996) as the result of the global seasonal pole-to-equator gradient (what we would name “large-scale upper

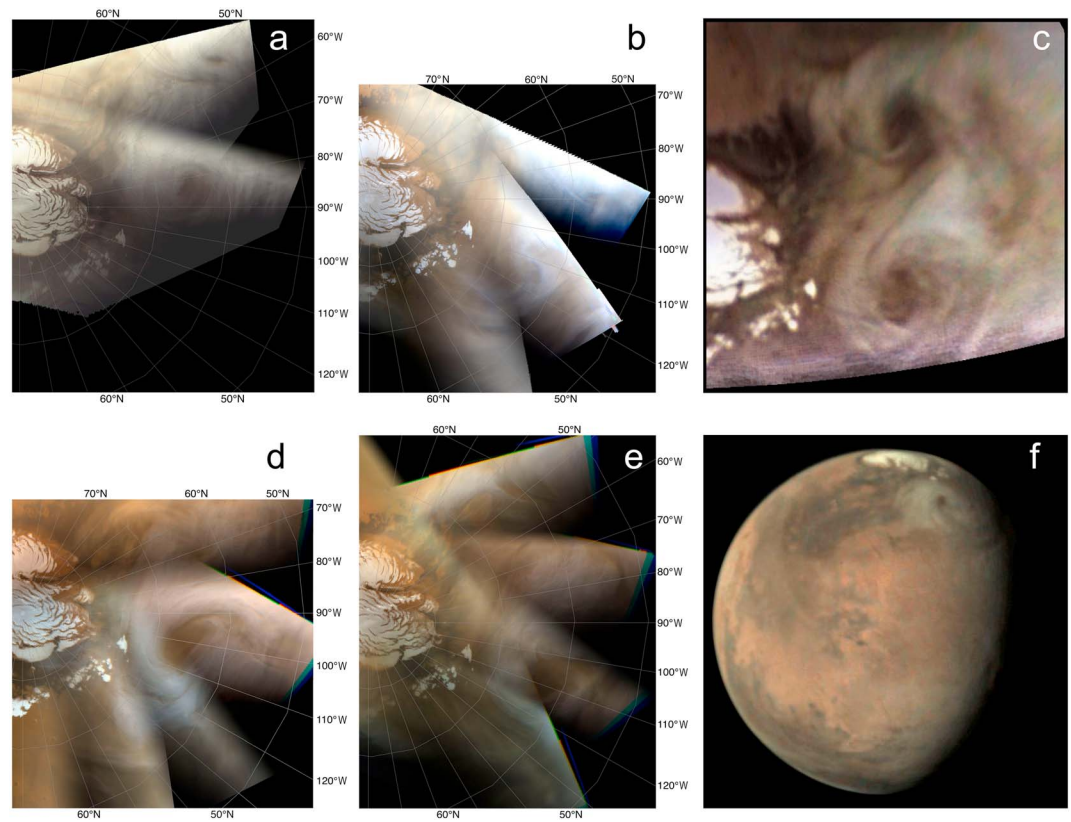


Figure 13. Selected images of the annular phenomenon as seen from different spacecraft showing its recurrence between 2008 and 2016 and its double nature at dawn in some cases. (a) MARCI/MRO, 25 September 2008, MY29 $L_s = 132.2^\circ$. (b) MARCI/MRO, 14 August 2010, MY30, $L_s = 132.5^\circ$. (c) VMC/MEx, 18 June 2012, MY25 $L_s = 126^\circ$. (d) MARCI/MRO, 1 May 2014, MY32 $L_s = 123.9^\circ$. (e) MARCI/MRO, 15 March 2016, MY33 $L_s = 122.5^\circ$. (f) VMC/MEx, 11 March 2016, M30 $L_s = 121^\circ$.

level baroclinicity”). The phenomenon described here is detected in summertime, where the large-scale upper level baroclinicity is known from modeling and observations to be particularly weak (Lewis et al., 2016). Thus, the kind of transient eddies that give rise to the polar cyclones described here at $L_s = 120^\circ$ are not related to large-scale upper level baroclinicity.

Transient eddies, often giving rise to “flushing” dust storms (Wang & Fisher, 2009), are also often observed during the advance and retreat of the seasonal CO_2 caps at both poles (e.g., Toigo & Richardson, 2002), in conditions we can describe as “lower level baroclinicity.” At the specific season of interest considered here (northern summer), there is no CO_2 seasonal cap in northern polar regions. Yet lower level baroclinicity caused by the thermal contrast between the bare soil of the surrounding plains and the northern polar residual cap made of water ice, albeit less pronounced than the contrast between bare soil and seasonal CO_2 ice caps, may still lead to transient eddies (Tyler & Barnes, 2005, 2014).

The phenomenon described here (see, e.g., Cantor et al., 2002; Hunt & James, 1979; Wang & Ingersoll, 2002) occurs as a combination of topographically driven thermal circulation, enhanced slope flows, and western boundary current effects along the equivalent of a storm zone at the longitude of Alba Patera (see detailed mesoscale modeling proposed by Tyler & Barnes, 2005, 2014). Through modeling and comparison with Phoenix measurements, Tyler and Barnes (2014) have already shown that the transient eddies in northern summer (associated with the recurring annular vortex cloud phenomenon) were indeed cyclonic vortices. The chaotic nature of the transients, and the interannual variability of dust loading in the polar regions, causes the transient eddies to be not repeatable in their properties from one Martian year to the other. This will be the subject of future work since it is well beyond the scope of the present paper and requires dedicated modeling studies.

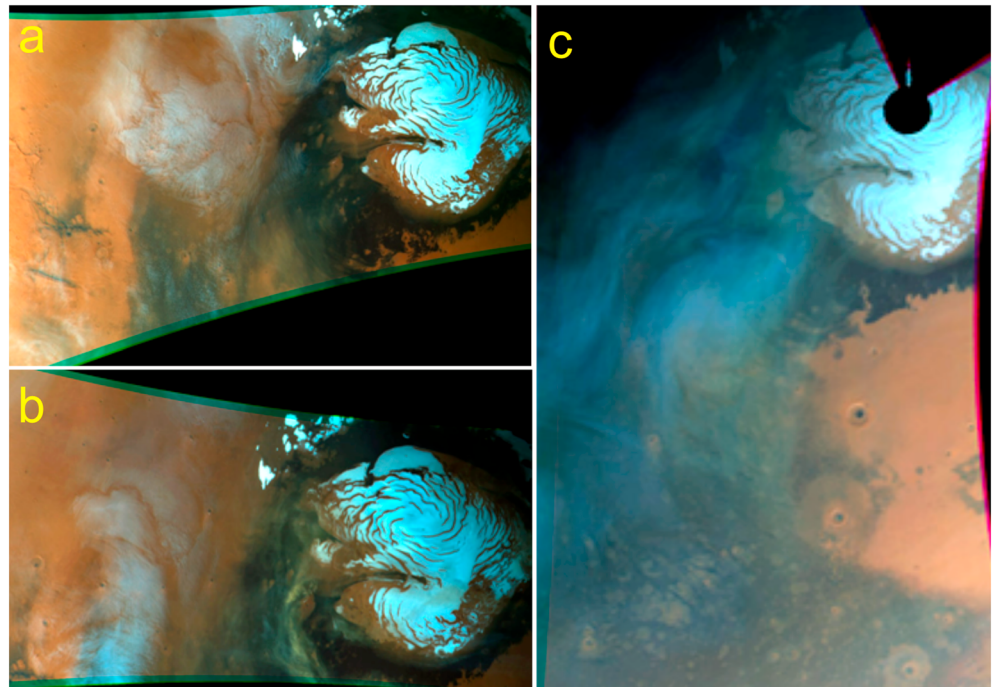


Figure 14. Images from HRSC-MEx showing snapshots of the cloud structure of the phenomenon in 2014 (see Table 2). (a) 02 May 2014, $L_s = 124.81$ (MEx orbit 13125). (b) 20 May 2014, $L_s = 133.19^\circ$ (MEx orbit 13185). (c) 15 June 2014, $L_s = 146.3^\circ$ (MEx orbit 13276). All images taken with HRSC push-broom mode with color composite RGB stretched. Push-broom observations are especially designed to avoid any parallax between the different color channels.

4. Conclusions

We have reported a study of the annular cloud phenomenon and the remarkable double cyclone (DC) that we have identified in some years, from detailed measurements in images obtained in 2012 and a survey of 1995–2018 images from a variety of sources. The feature forms recurrently every Martian year in the northern summer at $L_s = 120^\circ$ and areographical location at latitude $\sim 60^\circ\text{N}$ and longitudinal range $\sim 70^\circ\text{--}110^\circ\text{W}$. We have determined the properties of the double cyclone when present, and characterized its diurnal evolution. In the light of the present observational study, further modeling studies are necessary to address the following:

1. The delicate coupling of topographic and seasonal effects, described by Tyler and Barnes (2014), that gives rise to transient eddies in the summertime northern polar regions of Mars.
2. The peculiar conditions leading to the double-cyclone formation in some years and in this specific region as reported here and whether the variability we observe on it, is occurring randomly or coupled to a global interannual variability.
3. The evolution of the observed structures with local time and season.

An appropriate modeling effort to explain those structures shall employ either a mesoscale model with polar stereographic projection (as in Tyler & Barnes, 2005, 2014) or a high-resolution Global Climate Model devoid of the numerical singularity at the pole. A run lasting at least tens of Martian sols is necessary to capture a correct statistics of the transient eddies. The interannual changes shall also be explored with suitable dust scenarios accounting for atmospheric dust opacity variability (Montabone et al., 2015).

It would be of great interest to study the recurrent seasonal formation of the annular cloud phenomena and DC and analyze the changes in its properties each season (date of formation, location of its genesis, structure and intensity of each vortex, life cycle). This would allow to explore if it could be used as a reference to estimate the state of the atmosphere and, together with other cloud-forming recurrent dynamical phenomena, the interannual variability of the Martian atmosphere. Specifically, we propose to compare the properties of this dynamical system each MY with other known data of the Martian atmosphere for that same MY, for

example, the amount of dust, distribution and abundance of water vapor, evolution of the temperature, or the knowledge of the number, extent, and intensity of the development of dust storms before $L_s = 120^\circ$. We want to search for the interconnection between all these phenomena, looking for trends in relation to other interannual variations, as well as their modeling. The Mars Climate Database (MCD) of the Laboratoire de Météorologie Dynamique (Forget et al., 1999; Millour et al., 2015) will be used as a guide for this purpose. These aspects will be addressed in a future work.

Acknowledgments

This work has been supported by the Spanish project AYA2015-65041-P (MINECO/FEDER, UE) and Grupos Gobierno Vasco IT-765-13. H.C.C. and I.O.-E. were supported in part by Aula EspaZio Gela under contract from Diputación Foral de Bizkaia. A.G. was supported by ESA contract 4000118461/16/ES/JD, Scientific Support for Mars Express Visual Monitoring Camera. A.M. acknowledges funding from the French Space Agency CNES. All the images and data used in this study can be accessed through NASA PDS and ESA PSA Systems. A list of the sources for the images used in this paper can be found in the supporting information.

References

- Allison, M. (1997). Accurate analytic representations of solar time and seasons on Mars with applications to the pathfinder/surveyor missions. *Geophysical Research Letters*, *24*(16), 1967–1970. <https://doi.org/10.1029/97GL01950>
- Barnes, J. R. (1984). Linear baroclinic instability in the Martian atmosphere. *Journal of the Atmospheric Sciences*, *41*, 1536–1550.
- Barnes, J. R., Pollack, J. B., Haberle, R. M., Leovy, C. B., Zurek, R. W., Lee, H., & Schaeffer, J. (1993). Mars atmospheric dynamics as simulated by the NASA Ames general circulation model 2. Transient baroclinic eddies. *Journal of Geophysical Research*, *98*(E2), 3125–3148. <https://doi.org/10.1029/92JE02935>
- Bell, J. F., Wolff, M. J., Malin, M. C., Calvin, W. M., Cantor, B. A., Caplinger, M. A., et al. (2009). Mars reconnaissance Orbiter Mars Color Imager (MARCI): Instrument description, calibration and performance. *Journal of Geophysical Research*, *114*, E08S92. <https://doi.org/10.1029/2008JE003315>
- Bibring, J.-P., Soufflot, A., Berthé, M., Langevin, Y., Gondet, B., Drossart, P., et al. (2004). OMEGA: Observatoire pour la Minéralogie, l'Eau, les Glaces et l'Activité. In *Mars Express: The Scientific Payload*, Eur. Space Agency Spec. Publ., ESA-SP (Vol. 1240, pp. 37–50). Noordwijk, Netherlands: European Space Agency.
- Briggs, G. A., & Leovy, C. B. (1974). Mariner 9 observations of the Mars north polar hood. *Bulletin of the American Meteorological Society*, *55*(4), 278–296. [https://doi.org/10.1175/1520-0477\(1974\)055<0278:MOOTMN>2.0.CO;2](https://doi.org/10.1175/1520-0477(1974)055<0278:MOOTMN>2.0.CO;2)
- Cantor, B., Malin, M., & Edgett, K. S. (2002). Multiyear Mars Orbiter Camera (MOC) observations of repeated Martian weather phenomena during the northern summer season. *Journal of Geophysical Research*, *107*(E3), 5014. <https://doi.org/10.1029/2001JE001588>
- Clancy, R. D., Montmessin, F., Bension, J., Daerden, F., Colaprete, A., & Wolff, M. J. (2017). Mars clouds, in *The Atmosphere and Climate of Mars* (edited M. Haberle, R. T. Clancy, F. Forget, M. D. Smith, R. W. Zurek), Cambridge Univ. Press, Cambridge, UK, and New York.
- Forget, F., Hourdin, F., Fournier, R., Hourdin, C., Talagrand, O., Collins, M., Lewis, S. R., et al. (1999). Improved general circulation models of the Martian atmosphere from the surface to above 80 km. *Journal of Geophysical Research*, *104*(E10), 24,155–24,175. <https://doi.org/10.1029/1999JE001025>
- Garate-Lopez, I., Hueso, R., Sánchez-Lavega, A., Peralta, J., Piccioni, G., & Drossart, P. (2013). A chaotic long-lived vortex at the southern pole of Venus. *Nature Geoscience*, *6*(4), 254–257. <https://doi.org/10.1038/ngeo1764>
- Hollingsworth, J. L., Haberle, R. M., Barnes, J. R., Bridger, A. F. C., Pollack, J. B., Lee, H., & Schaeffer, J. (1996). Orographic control of storm zones on Mars. *Nature*, *380*(6573), 413–416. <https://doi.org/10.1038/380413a0>
- Holstein-Rathlou, C., Gunnlaugsson, H. P., Merrison, J. P., Bean, K. M., Cantor, B. A., Davis, J. A., Davy, R., et al. (2010). Winds at the Phoenix landing site. *Journal of Geophysical Research*, *115*, E00E18. <https://doi.org/10.1029/2009JE003411>
- Houze, R. A. (2014). *Cloud Dynamics, International Geophysics Series*, chap.5 & 6 (2nd ed., Vol. 53). San Diego: Academic Press.
- Hueso, R., Legarreta, J., García-Melendo, E., Sánchez-Lavega, A., & Pérez-Hoyos, S. (2009). The Jovian anticyclone BA. II. Circulation and interaction with the zonal jets. *Icarus*, *203*(2), 499–515. <https://doi.org/10.1016/j.icarus.2009.05.004>
- Hueso, R., Legarreta, J., Rojas, J. F., Peralta, J., Pérez-Hoyos, S., del Río Gaztelurrutia, T., & Sánchez-Lavega, A. (2010). The Planetary Laboratory for Image Analysis (PLIA). *Advances in Space Research*, *46*(9), 1120–1138. <https://doi.org/10.1016/j.asr.2010.05.016>
- Hunt, G. E., & James, P. B. (1979). Martian extratropical cyclones. *Nature*, *278*(5704), 531–532. <https://doi.org/10.1038/278531a0>
- Jaumann, R., Neukum, G., Behnke, T., Duxbury, T. C., Eichertopf, K., Flohrer, J., Gasselt, S., et al. (2007). The high-resolution stereo camera (HRSC) experiment on Mars express: Instrument aspects and experiment conduct from interplanetary cruise through the nominal mission. *Planetary and Space Science*, *55*(7-8), 928–952. <https://doi.org/10.1016/j.pss.2006.12.003>
- Lewis, S. R., Mulholland, D. P., Read, P. L., Montabone, L., Wilson, R. J., & Smith, M. D. (2016). The solstitial pause on Mars: 1. A planetary wave reanalysis. *Icarus*, *264*, 456–464. <https://doi.org/10.1016/j.icarus.2015.08.039>
- Madeleine, J. B., Forget, F., Millour, E., Navarro, T., & Spiga, A. (2012). The influence of radiatively active water ice clouds on the Martian climate. *Geophysical Research Letters*, *39*, L23202. <https://doi.org/10.1029/2012GL053564>
- Malin, M. C., Danielson, G. E., Ingersoll, A. P., Masursky, H., Veverka, J., Ravine, M. A., & Soulanille, T. A. (1992). The Mars observer camera. *Journal of Geophysical Research*, *97*(E5), 7699–7718. <https://doi.org/10.1029/92JE00340>
- Malin, M. C., Edgett, K. S., Cantor, B. A., Caplinger, M. A., Danielson, G. E., Jensen, E. H., Ravine, M. A., et al. (2010). An overview of the 1985–2006 Mars orbiter camera science investigation. *Mars*, *5*, 1–60. <https://doi.org/10.1555/mars.2010.0001>
- Millour, E., Forget, F., Spiga, A., Navarro, T., Madeleine, J. B., Montabone, L., Pottier, A., et al. (2015). The Mars Climate Database (MCD version 5.2). EPSC Abstracts, Vol. 10, EPSC2015-438.
- Montabone, L., Forget, F., Millour, E., Wilson, R. J., Lewis, S. R., Cantor, B., Kass, D., et al. (2015). Eight-year climatology of dust optical depth on Mars. *Icarus*, *251*, 65–95. <https://doi.org/10.1016/j.icarus.2014.12.034>
- Moores, J. E., Lemmon, M. T., Smith, P. H., Komguem, L., & Whiteway, J. A. (2010). Atmospheric dynamics at the Phoenix landing site as seen by the surface stereo imager. *Journal of Geophysical Research*, *115*, E00E08. <https://doi.org/10.1029/2009JE003409>
- Navarro, T., Madeleine, J. B., Forget, F., Spiga, A., Millour, E., Montmessin, F., & Määttänen, A. (2014). Global climate modeling of the Martian water cycle with improved microphysics and radiatively active water ice clouds. *Journal of Geophysical Research: Planets*, *119*, 1479–1495. <https://doi.org/10.1002/2013JE004550>
- Ormston, T., Denis, M., Skuza, D., & Griebel, H. (2011). An ordinary camera in an extraordinary location: Outreach with the Mars webcam. *Acta Astronautica*, *69*(7-8), 703–713. <https://doi.org/10.1016/j.actaastro.2011.04.015>
- Sánchez-Lavega, A. (2011). *An Introduction to Planetary Atmospheres*. Boca Raton, Florida: Taylor-Francis, CRC Press.
- Sánchez-Lavega, A., Chen-Chen, H., Ordoñez-Etxeberria, I., Hueso, R., del Río-Gaztelurrutia, T., Garro, A., Cardesín-Moinelo, A., et al. (2018). Limb clouds and dust on Mars from images obtained by the visual monitoring camera (VMC) onboard Mars express. *Icarus*, *299*, 194–205. <https://doi.org/10.1016/j.icarus.2017.07.026>
- Smith, P. H., Tamppari, L. K., Arvidson, R. E., Bass, D., Blaney, D., Boynton, W. V., Carswell, A., et al. (2009). H₂O at the Phoenix landing site. *Science*, *325*(5936), 58–61. <https://doi.org/10.1126/science.1172339>

- Spiga, A., Hinson, D. P., Madeleine, J.-P., Navarro, T., Millour, E., Forget, F., & Montmessin, F. (2017). Snow precipitation on Mars driven by cloud-induced night-time convection. *Nature Geoscience*, *10*(9), 652–657. <https://doi.org/10.1038/ngeo3008>
- Toigo, A. D., & Richardson, M. I. (2002). A mesoscale model for the Martian atmosphere. *Journal of Geophysical Research*, *107*(E7), 5049. <https://doi.org/10.1029/2000JE001489>
- Tyler, D. Jr., & Barnes, J. R. (2005). A mesoscale model study of summertime atmospheric circulations in the north polar region of Mars. *Journal of Geophysical Research*, *110*, E06007. <https://doi.org/10.1029/2004JE002356>
- Tyler, D. Jr., & Barnes, J. R. (2014). Atmospheric mesoscale modeling of water and clouds during northern summer on Mars. *Icarus*, *237*, 388–414. <https://doi.org/10.1016/j.icarus.2014.04.020>
- Wang, H., & Fisher, J. A. (2009). North polar frontal clouds and dust storms on Mars during spring and summer. *Icarus*, *204*(1), 103–113. <https://doi.org/10.1016/j.icarus.2009.05.028>
- Wang, H., & Ingersoll, A. P. (2002). Martian clouds observed by Mars global surveyor Mars orbiter camera. *Journal of Geophysical Research*, *107*(E10), 5078. <https://doi.org/10.1029/2001JE001815>
- Whiteway, J. A., Komguem, L., Dickinson, C., Cook, C., Illnicki, M., Seabrook, J., Popovici, V., et al. (2009). Mars water-ice clouds and precipitation. *Science*, *235*, 68–70.
- Wilson, R. J., Neumann, G. A., & Smith, M. D. (2007). Diurnal variation and radiative influence of Martian water ice clouds. *Geophysical Research Letters*, *34*, L02710. <https://doi.org/10.1029/2006GL027976>